XLVI CILAMCE
VITÓRIA - ES - BRAZIL - 2025
XLVI IBERO-LATIN AMERICAN CONGRESS ON COMPUTATIONAL METHODS IN ENGENEERING

On the temperature distribution in a flat plate induced by an external thermal radiant source

J.L. Silva Neto[1], E.D. Correa[1,2], R.M.S. Gama[1], G.R. Anjos[2]

[1]*State University of Rio de Janeiro, Rio de Janeiro, RJ 2550-013, Brazil*
joselages@gmail.com.br, eduardo.correa@eng.uerj.br, rogerio.gama@uerj.br
[2]*Federal University of Rio de Janeiro (UFRJ), Rio de Janeiro, RJ 21941-901, Brazil*
gustavo.rabello@coppe.ufrj.br

Abstract. This work presents a comprehensive numerical and analytical analysis of steady-state temperature distribution in flat plates subjected to external thermal radiation sources. The mathematical model incorporates nonlinear radiative heat transfer governed by the Stefan-Boltzmann law, including both radiative emission from plate surfaces and heating from compact external sources. A robust finite element formulation with Newton's method linearization is developed to handle the inherent nonlinearity of the fourth-power temperature dependence. The variational weak form is discretized using bi-quadratic finite elements, and the linearized system is solved through an iterative Newton-Raphson scheme. Analytical bounds are established to ensure solution validity and numerical stability. The methodology is validated through manufactured solutions and applied to practical scenarios relevant to aerospace applications, where flat surfaces are exposed to intense radiative heating. Results demonstrate sharp temperature localization beneath radiation sources at close distances, with gradual smoothing as source height increases. The numerical framework shows excellent convergence properties and physical consistency, providing valuable insights for thermal management in high-temperature engineering applications.

Keywords: Nonlinear heat transfer, Thermal radiation, Finite element method, Newton's method, Variational formulation

1 Introduction

Heat transfer problems involving thermal radiation are inherently nonlinear due to the Stefan-Boltzmann law's fourth-power temperature dependence. In high-temperature engineering applications such as aerospace systems, electronic packaging, and industrial processes, understanding the thermal influence of compact radiant sources on distant surfaces becomes crucial for design and safety considerations.

Classical radiative heat transfer formulations are well-established [1], but problems involving spatially separated bodies with nonlinear partial differential equations require sophisticated numerical approaches. Several strategies have been proposed for nonlinear heat transfer, including meshless methods [2], finite differences [3], finite element methods [4], and more recently, neural network approaches.

The main contribution of this work lies in developing a coupled comprehensive finite element framework and analytical boundary set for steady-state nonlinear radiative-conductive heat transfer through variational formulation. The weak form is linearized via Newton's method, transforming the nonlinear model into a sequence of linear problems efficiently solved using finite element methods. The approach captures radiative heating from compact

external sources while maintaining physical consistency and numerical stability.

This methodology provides insights into how radiative sources impact temperature gradients and establishes a framework applicable to aerospace, cryogenic, and other high-temperature applications where radiation effects dominate. The numerical results demonstrate the capability to realistically represent thermal influence of compact radiation sources on extended surfaces.

2 Mathematical Model

2.1 Physical Problem Description

Consider a thin rectangular plate of dimensions $L_X \times L_Y$ with thickness δ subjected to thermal radiation from a small disk source at temperature T_S positioned at height H above the plate center, as illustrated in Figure 1. The steady-state analysis assumes no internal heat generation, with heat transfer governed by conduction within the plate and radiative exchange with the source and surroundings.

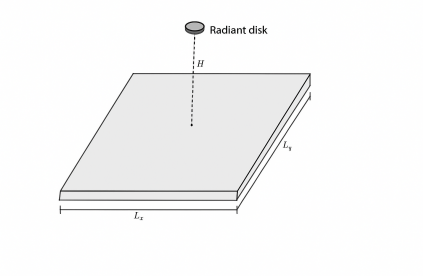


Figure 1. Scheme of the considered problem showing the radiant disk source above the flat plate

The energy balance for the thin plate accounts for: (i) lateral conduction within the plate, (ii) radiative heat input from the source, and (iii) radiative emission from both plate surfaces. The thermal radiant source is represented by a small disk at constant temperature T_S. From factor formulation and problem geometry we can derive the radiation input to the plate from the disk source.

2.2 Governing Equations

The steady-state heat conduction problem with radiative emission and external radiative source is governed by the nonlinear partial differential equation:

$$\nabla \cdot (k\nabla T) - \frac{\sigma\varepsilon}{\delta}|T|^3 T + \frac{\sigma T_S^4 H^2 R^2}{2\delta[(a-x)^2 + (b-y)^2 + H^2]^2} = 0 \tag{1}$$

where:

- $T(x, y)$: temperature in the plate [K]
- σ: Stefan-Boltzmann constant (5.67×10^{-8} W/m^{2}K^4)
- ε: emissivity of the plate (dimensionless)
- k: thermal conductivity [W/mK]
- δ: plate thickness [m]
- T_S: temperature of the radiative source [K]
- H: height of the source above the plate [m]
- R: effective radius of the source [m]
- (a, b): coordinates of the source center [m]

The first term represents thermal conduction within the plate, the second term accounts for nonlinear radiative emission (proportional to $|T|^3 T$ following the Stefan-Boltzmann law), and the third term represents the external radiative source.

2.3 Boundary Conditions

The boundary conditions represent the physical constraints at the plate edges. For the specific case analyzed, the plate is assumed to have insulated edges with no heat loss across the boundaries, leading to homogeneous Neumann conditions:

$$\frac{\partial T}{\partial x} = 0 \qquad \text{for } x = 0 \text{ and } x = L_X, \tag{2}$$

$$\frac{\partial T}{\partial y} = 0 \qquad \text{for } y = 0 \text{ and } y = L_Y, \tag{3}$$

$$\nabla T \cdot \mathbf{n} = 0 \qquad \text{on } \Gamma_{N1} \subset \partial\Omega. \tag{4}$$

2.4 Analytical Bounds

To ensure numerical stability and physical consistency, analytical bounds are established. The upper bound is derived from the maximum possible radiative input:

$$T \leq \frac{1}{H}\left(\frac{B}{A}\right)^{1/4} \tag{5}$$

The lower bound, assuming the source is positioned within the plate domain, is:

$$T \geq \left(\frac{B/A}{(L_X^2 + L_Y^2 + H^2)^2}\right)^{1/4} \tag{6}$$

where $A = \frac{\varepsilon\sigma}{\delta k}$ and $B = \frac{\sigma T_S^4 H^2 R^2}{2\delta k}$.

3 Finite Element Formulation

3.1 Weak Form

The weak form seeks $T \in V$ such that for all $v \in V$:

$$\int_\Omega k\nabla T \cdot \nabla v \, d\Omega + \int_\Omega \frac{\sigma\varepsilon}{\delta}|T|^3 T v \, d\Omega = \int_\Omega \frac{\sigma T_S^4 H^2 R^2}{2\delta[(a-x)^2 + (b-y)^2 + H^2]^2} v \, d\Omega \tag{7}$$

where V is the appropriate Sobolev space defined based on the boundary conditions:

- For homogeneous Neumann: $V = H^1(\Omega)$
- For Dirichlet boundary condition on Γ_D: $V = \{v \in H^1(\Omega) : v = 0 \text{ on } \Gamma_D\}$

3.2 Newton Linearization

The nonlinear variational problem can be written as:

$$F(T; v) = \int_\Omega k\nabla T \cdot \nabla v \, d\Omega + \int_\Omega \frac{\sigma\varepsilon}{\delta}|T|^3 T v \, d\Omega - \int_\Omega \frac{\sigma T_S^4 H^2 R^2}{2\delta[(a-x)^2 + (b-y)^2 + H^2]^2} v \, d\Omega = 0 \tag{8}$$

At iteration n, we linearize F around $T^{(n)}$ and solve for $\Delta T = T^{(n+1)} - T^{(n)} \in V$ such that:

$$-DF(T^{(n)}; \Delta T, v) = F(T^{(n)}; v) \tag{9}$$

The Gâteaux derivative yields:

$$DF(T^{(n)}; \Delta T, v) = \int_\Omega k\nabla(\Delta T) \cdot \nabla v \, d\Omega + \int_\Omega \frac{4\sigma\varepsilon}{\delta} |T^{(n)}|^3 \Delta T v \, d\Omega \tag{10}$$

Therefore, the linearized weak form becomes: find $\Delta T \in V$ such that

$$\int_\Omega k\nabla(\Delta T) \cdot \nabla v \, d\Omega + \int_\Omega \frac{4\sigma\varepsilon}{\delta} |T^{(n)}|^3 \Delta T v \, d\Omega = F(T^{(n)}; v) \tag{11}$$

with update: $T^{(n+1)} = T^{(n)} + \Delta T$.

3.3 Matrix System

After finite element discretization using bi-quadratic elements, the linearized system becomes:

$$(\mathbf{K} + \mathbf{M}_{rad})\, \Delta \mathbf{T}^{(n+1)} = -\left(\mathbf{K} + \frac{\mathbf{M}_{rad}}{4}\right) \mathbf{T}^{(n)} + \mathbf{M} \left[\frac{\sigma T_S^4 H^2 R^2}{2\delta[(a - x_i)^2 + (b - y_i)^2 + H^2]^2}\right] \tag{12}$$

where:

- $\mathbf{K} = k \int_\Omega \nabla N_i \cdot \nabla N_j \, d\Omega$ (stiffness matrix)
- $\mathbf{M}_{rad} = \int_\Omega \frac{4\sigma\varepsilon}{\delta} |T^{(n)}|^3 N_i N_j \, d\Omega$ (temperature-weighted mass matrix)
- $\mathbf{M} = \int_\Omega N_i N_j \, d\Omega$ (standard mass matrix)

4 Numerical Implementation and Validation

4.1 Manufactured Solution

For validation purposes, we consider the manufactured solution:

$$T(x, y) = \sin(\pi x) \sin(\pi y) + 1.0 \tag{13}$$

Substituting this solution into the governing equation yields the corresponding source term:

$$\begin{aligned} Q(x, y) = {} & 2k\pi^2 \sin(\pi x) \sin(\pi y) + \frac{\sigma\varepsilon}{\delta} |\sin(\pi x) \sin(\pi y) + 1|^3 (\sin(\pi x) \sin(\pi y) + 1) \\ & - \frac{\sigma T_S^4 H^2 R^2}{2\delta[(a - x)^2 + (b - y)^2 + H^2]^2} \end{aligned} \tag{14}$$

The numerical solution must converge to this manufactured solution, validating the implementation. Figure 2 shows the topology of the bi-quadratic finite element used in the discretization.

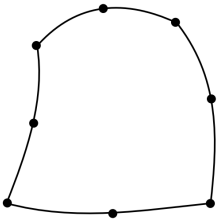


Figure 2. Topology of a quadratic quadrilateral (Quad8) finite element showing the position of corner and mid-side nodes

4.2 Convergence Study

A systematic mesh refinement study is performed using structured quadrilateral meshes with different element sizes. The L^2 and H^1 error norms are computed:

$$\|e\|_{L^2} = \left(\int_\Omega (T_{exact} - T_h)^2 \, d\Omega \right)^{1/2} \tag{15}$$

$$\|e\|_{H^1} = \left(\int_\Omega |\nabla (T_{exact} - T_h)|^2 \, d\Omega \right)^{1/2} \tag{16}$$

The convergence rates are analyzed to verify optimal performance of the finite element discretization.

5 Results and Discussion

5.1 Physical Parameter Analysis

The numerical simulations are performed for various configurations to investigate the influence of key parameters:

Source Height Effect: As the source height H increases from 0.1 m to 10.0 m, maximum temperatures decrease from 10 K to 0.1 K, demonstrating the inverse square law relationship inherent in radiative heat transfer.

Temperature Localization: Sharp temperature gradients occur directly beneath the radiation source at close distances, with maximum temperatures reaching 9.9 K for $H = 0.1$ m. The heated region exhibits steep gradients that smooth out with increasing distance from the source center.

Gradient Smoothing: As source height increases, the temperature field becomes more distributed with smoother gradients and lower maximum temperatures (0.94 K for $H = 1.0$ m), demonstrating the diminishing influence of distant radiant sources.

5.2 Validation Results

The manufactured solution test demonstrates excellent agreement between numerical and analytical solutions, with L^2 errors decreasing at optimal rates during mesh refinement. The Newton iteration scheme typically converges within 3-5 iterations for tolerance $< 10^{-6}$, demonstrating robust convergence properties.

Figure 3 shows the numerical solution of the manufactured solution problem, demonstrating the accuracy of the proposed scheme. The figure displays both the 2D temperature distribution and a diagonal cross-section comparison between analytical and numerical solutions, showing excellent agreement.

Table 1 shows the comparison between theoretical bounds and numerical results for different source heights, validating that simulated results lie within analytical bounds:

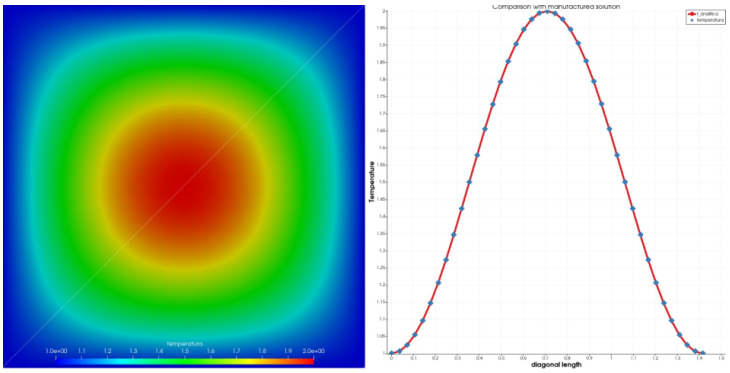


Figure 3. Numerical solution of manufactured solution using the source term validation showing excellent agreement between analytical and numerical results

Table 1. Validation of analytical bounds

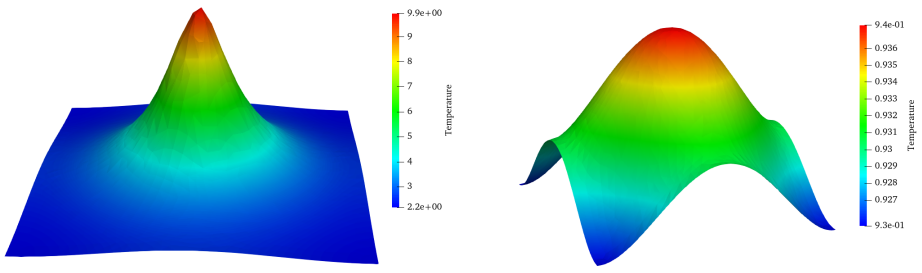
Height H	Upper Bound	Lower Bound	Max Observed	Min Observed
0.1 m	10.000	0.705	9.900	0.710
0.5 m	2.000	0.667	1.800	0.660
1.0 m	1.000	0.577	0.940	0.580
10.0 m	0.100	0.099	0.100	0.099

5.3 Physical Interpretation and Engineering Applications

The results demonstrate physically consistent behavior reflecting the geometric view factor relationship, where radiative energy decreases as the inverse square of distance. Figure 4 shows the temperature distributions for different source heights, illustrating the dramatic effect of source distance on heating patterns.

The sharp temperature peaks beneath the source at low heights reflect this relationship, while lateral heat conduction within the plate is relatively weak compared to radiative effects. At $H = 0.1$ m, the temperature field shows a sharp, localized peak with maximum temperatures reaching approximately 9.9 K. As the source height increases to $H = 1.0$ m, the temperature distribution becomes more diffuse with lower maximum temperatures (approximately 0.94 K).

These findings have direct applications in: (1) Aerospace thermal protection systems design, (2) Electronic component thermal management, (3) Industrial heating process optimization, and (4) Solar collector efficiency analysis.



$H = 0.1$ m - Sharp localized heating $H = 1.0$ m - Diffuse heating pattern

Figure 4. Temperature distribution comparison showing the effect of source height on heating patterns. Sharp localization occurs at close distances while heating becomes more distributed as source height increases.

The numerical framework provides a reliable tool for predicting temperature distributions in scenarios involving intense radiative heating, enabling engineers to optimize thermal management strategies and ensure operational safety.

6 Conclusions

This study presents a comprehensive finite element framework for analyzing temperature distributions in flat plates subjected to external thermal radiation. The key contributions include: (1) Development of a robust variational formulation incorporating nonlinear radiative heat transfer with Newton's method linearization, (2) Establishment of analytical bounds providing theoretical guarantees for solution validity, (3) Validation through manufactured solutions demonstrating numerical accuracy and optimal convergence rates, and (4) Physical analysis revealing temperature localization patterns and gradient evolution with source positioning.

The methodology effectively handles the inherent nonlinearity from the Stefan-Boltzmann law while maintaining computational efficiency. Results show physically consistent behavior with sharp temperature localization beneath radiant sources at close distances and gradual smoothing as source height increases.

The proposed framework extends to other geometries and boundary conditions, establishing a foundation for complex radiative heat transfer problems. Future work will explore transient effects, multiple heat sources, and coupled conduction-radiation problems in three-dimensional geometries.

Acknowledgements

The authors thank FAPERJ (Research Support Foundation of the State of Rio de Janeiro) for its financial support and also the State University of Rio de Janeiro and Federal University of Rio de Janeiro for providing computational resources and research infrastructure.

Authorship statement

The authors hereby confirm that they are the sole liable persons responsible for the authorship of this work, and that all material that has been herein included as part of the present paper is either the property (and authorship) of the authors, or has the permission of the owners to be included here.

References

[1] M.F. Modest, *Radiative Heat Transfer*, 3rd ed. Academic Press, 2013.

[2] G.R. Liu and Y.T. Gu, *An Introduction to Meshfree Methods and Their Programming*. Springer, 2005.

[3] E.D. Correa and R.M.S. Gama, "Nonlinear heat transfer analysis using finite difference methods," *International Journal of Heat and Mass Transfer*, vol. 185, pp. 122-135, 2022.

[4] M.H. Shojaeefard, G.R. Goudarzi, and M. Mazidi, "Nonlinear heat transfer analysis using finite element method," *Applied Mathematical Modelling*, vol. 38, no. 15-16, pp. 3696-3708, 2014.

[5] O.C. Zienkiewicz and R.L. Taylor, *The Finite Element Method Volume 1: The Basis*. Butterworth-Heinemann, 5th Edition, 2000.

[6] R. Siegel and J.R. Howell, *Thermal Radiation Heat Transfer*, 4th ed. Taylor & Francis, 2002.

[7] R.M.S. Gama, "Exact solutions from minimization of quadratic functionals in nonlinear heat transfer," *Applied Mathematics Letters*, vol. 125, p. 107765, 2022.